

> REPLACE THIS LINE WITH YOUR MANUSCRIPT ID NUMBER (DOUBLE-CLICK HERE TO EDIT) <

A Stability Analysis Tool for Bulk Power Systems Using Black-Box Models of Inverter-based Resources

Dongsen Sun, Hanchao Liu, Maozhong Gong, Zhe Chen, and Philip Hart

Abstract—This paper presents a small-signal stability analysis tool for large-scale power systems with high penetration of inverter-based resources (IBRs). Firstly, a network transfer function matrix (NTFM), which represents the information of the system topology, transmission lines, loads, IBRs locations, etc., is derived to model the entire power system network. Secondly, small-signal perturbation method is applied to obtain the sequence impedance/admittance models of the block-box IBRs considering the frequency cross-coupling effects. With the obtained NTFM as well as IBR models, a multi-input, multi-output (MIMO) feedback system is constructed, and the generalized Nyquist criterion (GNC)-based stability method is employed to analyze the stability of the entire power system. Furthermore, based on the developed stability analysis method, sensitivity analysis is conducted on an unstable case to identify which parameter has a high impact on the system stability. Different test cases based on a modified IEEE 14-bus system as well as a reduced 240-bus WECC system are studied to verify the proposed stability analysis tool.

Index Terms—Black-box model, generalized Nyquist criterion (GNC), Inverter-based resources (IBRs), stability analysis, sensitivity analysis

I. INTRODUCTION

Modern power systems have a large share of distribution energy resources (DERs), such as renewables, electrical vehicles, energy storage, etc. As most DERs are interfaced to the grid by inverters, these resources are also referred as inverter-based resources (IBRs). Due to characteristics of the power electronics-based systems such as low inertia as well as complex dynamics, the increased IBR integrations can induce stability issues for the entire power system. As described in [1], the IBRs may cause oscillations in the system with a wide range of frequencies, which eventually jeopardizes the entire system's stable operation.

One conventional oscillation analysis method used for traditional power systems is modal analysis, which uses the state-space model of the power system and extracts its eigenvalues and eigenvectors to identify the oscillatory modes as well as participation factors [2]-[4]. The modal analysis method is also applied to modern power systems containing IBRs. For instance, Ding in [5] conducted the stability analysis of low-inertia power grid, Zhou in [6] studied the power system

under uncertain renewable generations, and Pan in [7] identified the stability region of power systems under some perturbations. In addition, based on the eigenvalue sensitivity analysis, the impacts of different system parameters on system stability can be identified [8]-[10]. However, the modal analysis method has some challenges when applied to the modern power system with a high penetration of IBRs. On one hand, the system state-space model would feature a high order due to the complex dynamics of IBRs; furthermore, the modal analysis needs the open-box model of the IBRs, i.e., having the knowledge of control schemes as well as all parameters of IBRs, which would be impossible as most manufacturers would only provide the black-box models of IBRs and would not disclose its control system architecture and parameters.

The impedance-based stability-analysis method, which was originally applied to design the DC/DC converters in [11], has been proven to be an effective stability analysis method for interconnected systems. In recent years, many efforts have been focusing on developing the impedance-based methods to analyze the stability of power systems with IBRs [12]-[16]. Most existing works simplify the system to a point-to-point connection system, i.e., source-load system, and apply Nyquist criterion-based methods to analyze the system's stability [12]-[14]. Y. Li et al. [15] proposed a stability analysis and location optimization method for multi-converter power systems. W. Cao [16] proposed a component connection method to model multi-bus power systems and converted the system to a multi-input, multi-out (MIMO) system for stability analysis.

Likewise, most of the existing impedance-based stability-analysis methods have been applied to system models containing an open-box representation of IBRs. N. Cifuentes et al. [17] proposed a black-box impedance-based method to assess the stability and dynamic interactions for a 39-bus power system. However, in the stability analysis, rather than using the black-box model directly, a space-space model is employed, which is obtained by a linear time-invariant vector fitted from the black-box model. This technique could potentially compromise the accuracy of the analysis. Therefore, there is still no effective impedance-based stability analysis method for bulk power systems that maximally preserves the accuracy of the analysis by dealing with the black-box models of the IBRs directly.

This work is supported by the U.S. Department of Energy's Office of Energy Efficiency and Renewable Energy (EERE) under the Solar Energy Technologies Office Award Number DE-EE0009024.

> REPLACE THIS LINE WITH YOUR MANUSCRIPT ID NUMBER (DOUBLE-CLICK HERE TO EDIT) <

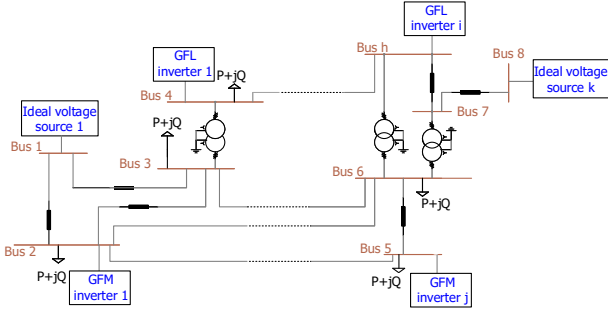


Fig. 1. An example power system network with multiple IBRs.

Moreover, eigenvalue sensitivity analysis has been applied to both traditional multi-machine power system analysis [18] and IBRs system analysis [19]. It can provide insights into the root cause of the system oscillations. However, these previous works are based on the detailed analytical model of power systems and IBRs and they are not applicable to integration studies when only black-boxed models of IBR are available.

To fill the technical gaps discussed above, the main contributions made by this paper are summarized as follows.

1) This paper presents a small-signal stability analysis tool for bulk power systems with a high-level integration of IBRs, based on the previous work [20]. The proposed tool directly uses the measured sequence impedance models of black-box IBRs, which reduces the implementation complexity and improves the accuracy of the system stability analysis.

2) Moreover, this paper proposes a numerical eigenvalue sensitivity analysis method, which can help to identify which IBRs or network parameters are the root causes of the system instability. The proposed sensitivity analysis is based on the measured sequence impedance models of black-box IBRs without knowing their control details or propriety information.

The remainder of this paper is organized as follows. Section II presents the detailed small-signal modeling of the power systems including the network transfer function matrix (NTFM) as well as the black-box models of IBRs (including models of grid-forming (GFM) and grid following (GFL) inverters). Section III presents how the stability analysis and sensitivity analysis are conducted in bulk power systems with IBRs. Section IV shows cases study and validates the effectiveness of the proposed methods. Finally, Section V summarizes the paper and draws the conclusions.

II. MODELING OF POWER SYSTEMS WITH IBRS

A. Modeling of the Power System Network

Fig. 1 shows the configuration of a generic power system, in which there are h buses interconnected by transmission lines or transformers. In the system, there are multiple IBRs (k GFL IBRs and j GFM IBRs), and multiple traditional generators (simplified to i ideal voltage sources (IVS)) attached to different buses.

The NTFM $\mathbf{G}_{nw}(s)$ of the power system is derived in this section and the detailed derivation procedure is shown as a flowchart in Fig. 2. Firstly, the specification of the power system network,

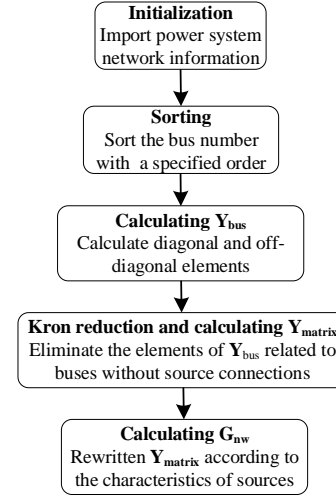


Fig. 2. Flow chart of calculating NTFM \mathbf{G}_{nw} .

including power rating, voltage rating, loads, transmission lines, source on each bus, is imported and initialized from input files. Then, $\mathbf{Y}_{bus}(s)$ is generated with a special order per the characteristic of the source on each bus. In this paper, the GFM and GFL inverters are modeled as Thevenin equivalent voltage sources and Norton equivalent current sources, respectively. Thus, there is

$$\mathbf{I} = \mathbf{Y}_{bus}(s) \mathbf{V} \quad (1)$$

where \mathbf{V} is the bus voltage vector (note that the bus voltage vector follows this bus order: buses with IVSs, GFM IBRs, GFL IBRs, and other buses); \mathbf{I} is the current vector, which represents the current injected to each bus and has the same order as \mathbf{V} . Note that the loads on the buses are converted to admittance models during obtaining the corresponding elements of $\mathbf{Y}_{bus}(s)$.

Moreover, $\mathbf{Y}_{bus}(s)$ should be expressed in a positive and negative sequence format to be compatible with the sequence impedance/admittance model of IBRs in the following section. There is

$$\mathbf{Y}_{bus}(s) = \begin{bmatrix} \mathbf{Y}_{pp11} & \mathbf{Y}_{pn11} & \mathbf{Y}_{pp12} & \mathbf{Y}_{pn12} & \cdots & \cdots \\ \mathbf{Y}_{np11} & \mathbf{Y}_{nn11} & \mathbf{Y}_{np12} & \mathbf{Y}_{nn12} & \cdots & \cdots \\ \mathbf{Y}_{pp21} & \mathbf{Y}_{pn21} & \cdots & \cdots & \cdots & \cdots \\ \mathbf{Y}_{np21} & \mathbf{Y}_{nn21} & \cdots & \cdots & \cdots & \cdots \\ \cdots & \cdots & \cdots & \cdots & \cdots & \cdots \\ \cdots & \cdots & \cdots & \cdots & \cdots & \cdots \end{bmatrix} \quad (2)$$

where subscripts p and n denote the positive and negative sequence, respectively. \mathbf{Y}_{ppmn} , \mathbf{Y}_{pnmn} , \mathbf{Y}_{npmn} , and \mathbf{Y}_{nnmn} are the positive and negative sequence components of the mn^{th} element of \mathbf{Y}_{bus} , respectively.

To eliminate the elements of \mathbf{Y}_{bus} related to the buses without source connected, Kron reduction [16], [21] needs to be conducted on \mathbf{Y}_{bus} . Firstly, equation (1) is rewritten as

$$\begin{bmatrix} \mathbf{I}_m \\ \mathbf{I}_n \end{bmatrix} = \begin{bmatrix} \mathbf{Y}_{mm}(s) & \mathbf{Y}_{mn}(s) \\ \mathbf{Y}_{nm}(s) & \mathbf{Y}_{nn}(s) \end{bmatrix} \begin{bmatrix} \mathbf{V}_m \\ \mathbf{V}_n \end{bmatrix} \quad (3)$$

where subscripts m and n represent the buses with and without source, respectively.

> REPLACE THIS LINE WITH YOUR MANUSCRIPT ID NUMBER (DOUBLE-CLICK HERE TO EDIT) <

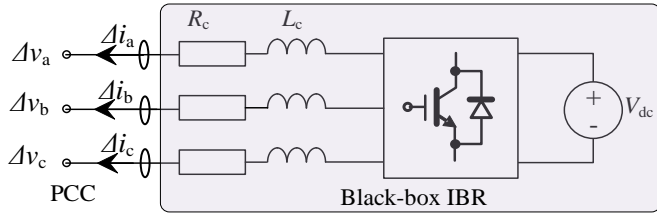


Fig. 3. Schematic diagram of small-signal perturbation method to measure the black-box IBR model.

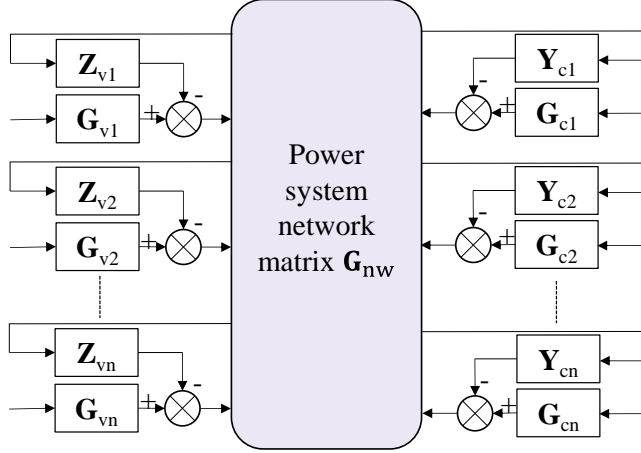


Fig. 4. Constructed the MIMO feedback system.

After conducting the Kron reduction, there is

$$\mathbf{I}_m = \mathbf{Y}_{\text{matrix}}(s) \mathbf{V}_m \quad (4)$$

$$\mathbf{Y}_{\text{matrix}}(s) = \mathbf{Y}_{mm}(s) - \mathbf{Y}_{mn}(s) \mathbf{Y}_{nn}(s)^{-1} \mathbf{Y}_{nm}(s) \quad (5)$$

According to the characteristic of the source on each bus, equation (4) is rewritten as

$$\begin{bmatrix} \mathbf{I}_v \\ \mathbf{I}_c \end{bmatrix} = \begin{bmatrix} \mathbf{Y}_{vv}(s) & \mathbf{Y}_{vc}(s) \\ \mathbf{Y}_{cv}(s) & \mathbf{Y}_{cc}(s) \end{bmatrix} \begin{bmatrix} \mathbf{V}_v \\ \mathbf{V}_c \end{bmatrix} \quad (6)$$

where subscripts v and c denote the buses with voltage source and current source, respectively.

Finally, $\mathbf{G}_{nw}(s)$ is obtained as

$$\begin{bmatrix} \mathbf{I}_v \\ \mathbf{V}_c \end{bmatrix} = \mathbf{G}_{nw}(s) \begin{bmatrix} \mathbf{V}_v \\ \mathbf{I}_c \end{bmatrix} \quad (7)$$

$$\mathbf{G}_{nw}(s) = \begin{bmatrix} \mathbf{Y}_{vv} & -\mathbf{Y}_{vc} \mathbf{Y}_{cc}^{-1} \mathbf{Y}_{cv} & \mathbf{Y}_{vc} \mathbf{Y}_{cc}^{-1} \\ -\mathbf{Y}_{cc}^{-1} \mathbf{Y}_{cv} & & \mathbf{Y}_{cc}^{-1} \end{bmatrix} \quad (8)$$

B. Black-box Model of IBRs

As the IBRs in the power system network are mostly black boxes without detailed internal information, it is necessary to obtain their impedance/admittance models using a measurement method. Moreover, considering the frequency cross-coupling effect, the sequence impedance/admittance models of the IBRs should be obtained.

The schematic diagram of the measurement method is shown in Fig. 3, in which small-signal positive and negative voltage perturbations with different frequency are applied at the point of common coupling (PCC) between the IBR and its connecting bus [21]. The response current, which is corresponding to the applied voltage perturbations can be

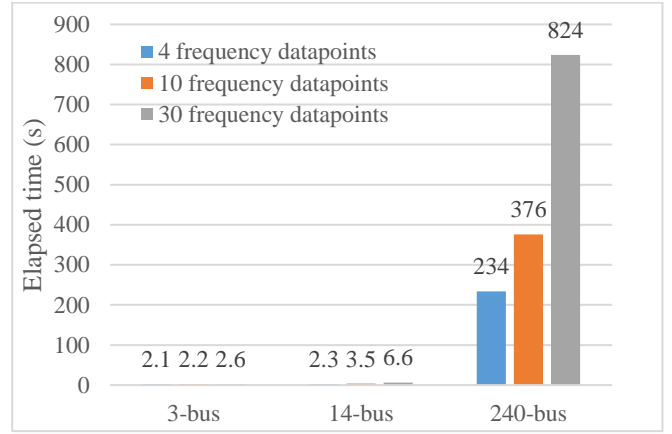


Fig. 5. Computation time comparison of different size system.

measured, and then using a fast Fourier transform (FFT) calculation, the impedance/admittance model of GFM/ GFL inverter can be obtained [22], [23].

To be specific, the sequence impedance model can be described as

$$\begin{bmatrix} \Delta \mathbf{v}_p(s + j\omega_1) \\ \Delta \mathbf{v}_n(s - j\omega_1) \end{bmatrix} = \begin{bmatrix} \mathbf{Z}_{pp} & \mathbf{Z}_{pn} \\ \mathbf{Z}_{np} & \mathbf{Z}_{nn} \end{bmatrix} \begin{bmatrix} \Delta \mathbf{i}_p(s + j\omega_1) \\ \Delta \mathbf{i}_n(s - j\omega_1) \end{bmatrix} \quad (9)$$

where, ω_1 is the fundamental angular frequency, $\Delta \mathbf{v}_p(s + j\omega_1)$ and $\Delta \mathbf{v}_n(s - j\omega_1)$ represent the positive and negative sequence perturbation voltage, respectively. $\Delta \mathbf{i}_p(s + j\omega_1)$ and $\Delta \mathbf{i}_n(s - j\omega_1)$ represent the positive and negative sequence perturbation current, respectively.

Likewise, the sequence admittance model can be obtained using the similar procedure. Thus, the measured black-box model of GFM and GFL inverters can be expressed as

$$\mathbf{Z}_v(s) = \begin{bmatrix} \mathbf{Z}_{pp} & \mathbf{Z}_{pn} \\ \mathbf{Z}_{np} & \mathbf{Z}_{nn} \end{bmatrix} \quad (10)$$

$$\mathbf{Y}_c(s) = \begin{bmatrix} \mathbf{Y}_{pp} & \mathbf{Y}_{pn} \\ \mathbf{Y}_{np} & \mathbf{Y}_{nn} \end{bmatrix} \quad (11)$$

where $\mathbf{Z}_{pp}(\mathbf{Y}_{pp})$, $\mathbf{Z}_{pn}(\mathbf{Y}_{pn})$, $\mathbf{Z}_{np}(\mathbf{Y}_{np})$, and $\mathbf{Z}_{nn}(\mathbf{Y}_{nn})$ are the corresponding positive and negative sequence impedance (admittance) components, respectively.

III. STABILITY ANALYSIS OF THE POWER SYSTEM

A. Impedance-based Stability Analysis

With the obtained system network model $\mathbf{G}_{nw}(s)$ as well as all the IBR models, a MIMO feedback system is constructed as shown in Fig. 4. In the figure, $\mathbf{G}_{vn}(s)$ and $\mathbf{G}_{cn}(s)$ are the closed-loop gain of the equivalent voltage source (GFM IBRs or IVS) and current source (GFL inverter based IBRs), respectively. Moreover, $\mathbf{Z}_{vn}(s)$ and $\mathbf{Y}_{cn}(s)$ represent the measured output impedance of GFM inverter (or IVS) and the measured output admittance of GFL inverter, respectively.

Writing all the measured models of the IBRs as a matrix, there is

$$\mathbf{G}_{cd}(s) = \text{diag}[\mathbf{Z}_{v1}, \dots, \mathbf{Z}_{vn}, \mathbf{Y}_{c1}, \dots, \mathbf{Y}_{cn}] \quad (12)$$

> REPLACE THIS LINE WITH YOUR MANUSCRIPT ID NUMBER (DOUBLE-CLICK HERE TO EDIT) <

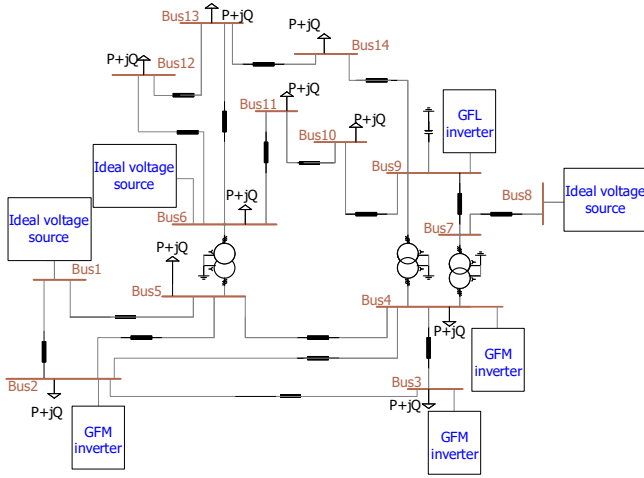


Fig. 6. A modified IEEE 14-bus power system with multiple IBRs.

Moreover, to conduct stability analysis of the MIMO feedback system, the return-ratio matrix $\mathbf{L}(s)$ and the return-difference matrix $\mathbf{F}(s)$ are defined as

$$\mathbf{L}(s) = \mathbf{G}_{cd}(s) \mathbf{G}_{nw}(s) \quad (13)$$

$$\mathbf{F}(s) = \mathbf{I} + \mathbf{L}(s) \quad (14)$$

According to the GNC, the stability of the constructed MIMO system can be analyzed by two methods, one is the determinant-based method, and the other is the eigenvalue-based method.

Defining that \mathbf{Z} is the number of zeros of $\mathbf{F}(s)$, \mathbf{P} is the number of right-half-plane (RHP) poles of $\mathbf{L}(s)$, and \mathbf{N} is the number of clockwise encirclements of the critical point $((0, j0)$ for determinant-based method and $(-1, j0)$ for eigenvalue-based method), according to the GNC [16], [25], there is

$$\mathbf{Z}(\mathbf{F}) = \mathbf{P}(\mathbf{L}) + \mathbf{N}(\mathbf{L}) \text{ or } \mathbf{Z}(\mathbf{F}) = \mathbf{P}(\mathbf{L}) + \mathbf{N}(\det(\mathbf{F})) \quad (15)$$

As the power system network consists only passive components, there is no RHP poles on $\mathbf{G}_{nw}(s)$. Moreover, all the IBRs are designed to be stable when operating separately, so there is no RHP poles on $\mathbf{G}_{cd}(s)$. Therefore, $\mathbf{L}(s)$ does not have any RHP poles, i.e., $\mathbf{P}(\mathbf{L})=0$. Thus, the system is stable if and only if

- 1) the Nyquist plot of $\det(\mathbf{F}(s))$ does not encircle critical point $(0, j0)$ clockwise.
- 2) the Nyquist plots of all the eigenvalue of $\mathbf{L}(s)$ do not encircle critical point $(-1, j0)$ clockwise.

Furthermore, to increase the computation speed, the stability analysis tool is implemented in Matlab in a numerical way, which means all the operation of matrices are conducted at each frequency point. The specification of the computer used to implement the stability analysis is Intel(R) Core(TM) i7-10850H CPU @ 2.70GHz 2.71 GHz. To compare the computation time, stability analysis is conducted on three different size systems, i.e., 3-bus, 14-bus, and 240-bus system, and different number of the frequency datapoints are analyzed. The comparison result is shown in Fig. 5. It is observed that the stability analysis could be completed very fast when applies to

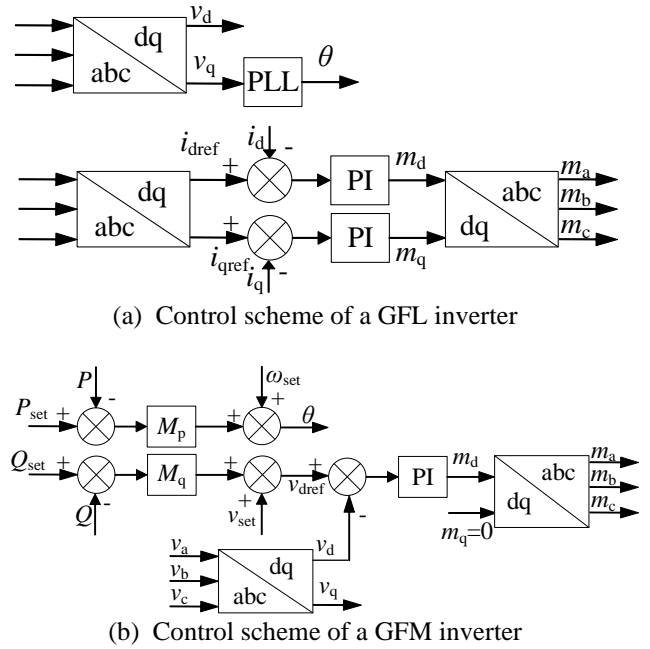


Fig. 7. Control scheme of IBRs in the power system

a small system, and the computation time increases with the increase of the size of the system and the number of the frequency datapoints. However, it is still acceptable to complete the stability analysis of a 240-bus system within 14 minutes. The optimization on the stability tool as well as the upgrade of the computer would further increase its computation speed in future.

B. Sensitivity Analysis

The stability analysis method proposed in the previous section could predict if the system is stable or not, and the eigenvalues of $\mathbf{L}(s)$ could further predict instability modes and their stability margin. Moreover, in this section, a numerical sensitivity analysis method is proposed to identify the sensitivity of the resonant modes to different system components. With the sensitivity analysis, we can identify which bus or branch impedances is dominating the resonance mode and causing the system instability.

In the eigenvalue-based stability method, the eigenvalues of return-ratio matrix $\mathbf{L}(s)$ are used to determine the system stability. Furthermore, the sensitivity of the eigenvalues of $\mathbf{L}(s)$ on each element of \mathbf{G}_{cd} and \mathbf{G}_{nw} , can be used to quantify the sensitivity of the system resonant modes with respect to system components. Assume λ_n is the n^{th} eigenvalue of matrix \mathbf{L} , there are

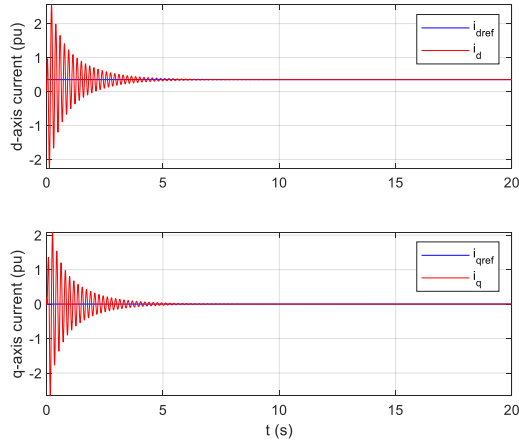
$$\frac{\partial \mathbf{L}}{\partial \mathbf{G}_{cdij}} = u_n^T \frac{\partial \mathbf{G}_{cd}}{\partial \mathbf{G}_{cdij}} \mathbf{G}_{nw} w_n + u_n^T \mathbf{G}_{cd} \frac{\partial \mathbf{G}_{nw}}{\partial \mathbf{G}_{cdij}} w_n \quad (16)$$

$$\frac{\partial \mathbf{L}}{\partial \mathbf{G}_{nwij}} = u_n^T \frac{\partial \mathbf{G}_{cd}}{\partial \mathbf{G}_{nwij}} \mathbf{G}_{nw} w_n + u_n^T \mathbf{G}_{cd} \frac{\partial \mathbf{G}_{nw}}{\partial \mathbf{G}_{nwij}} w_n \quad (17)$$

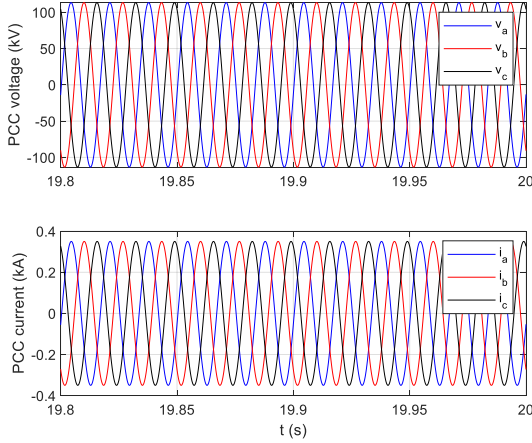
where u_n and w_n are the n^{th} left and right eigenvector of \mathbf{L} and

$$\frac{\partial \mathbf{G}_{nw}}{\partial \mathbf{G}_{cdij}} = \frac{\partial \mathbf{G}_{cd}}{\partial \mathbf{G}_{nwij}} = 0 \quad (18)$$

> REPLACE THIS LINE WITH YOUR MANUSCRIPT ID NUMBER (DOUBLE-CLICK HERE TO EDIT) <



(a) d- and q-axis currents.



(b) Voltage and current at PCC.

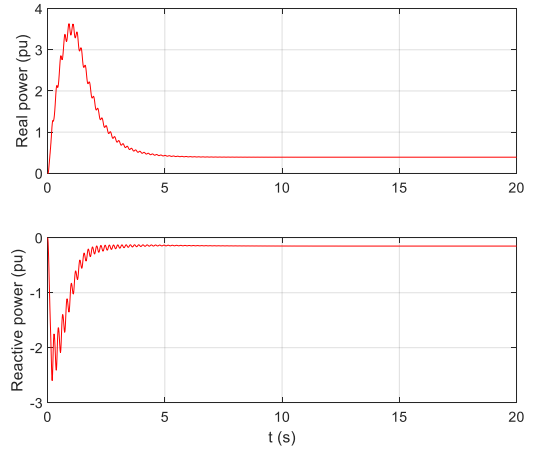
Fig. 12. PSCAD simulation result of GFL inverter on Bus 9.

Therefore, $\frac{\partial \mathbf{L}}{\partial \mathbf{G}_{cdij}} = \mathbf{u}_n^T \frac{\partial \mathbf{G}_{cd}}{\partial \mathbf{G}_{cdij}} \mathbf{G}_{nw} \mathbf{w}_n$ will be the matrix that represents the sensitivity of each element \mathbf{G}_{nw} on the n^{th} eigenvalue of \mathbf{L} and $\frac{\partial \mathbf{L}}{\partial \mathbf{G}_{nwi}} = \mathbf{u}_n^T \mathbf{G}_{cd} \frac{\partial \mathbf{G}_{nw}}{\partial \mathbf{G}_{nwi}}$ will be the matrix that represents the sensitivity of each element \mathbf{G}_{cd} on the n^{th} eigenvalue of \mathbf{L} .

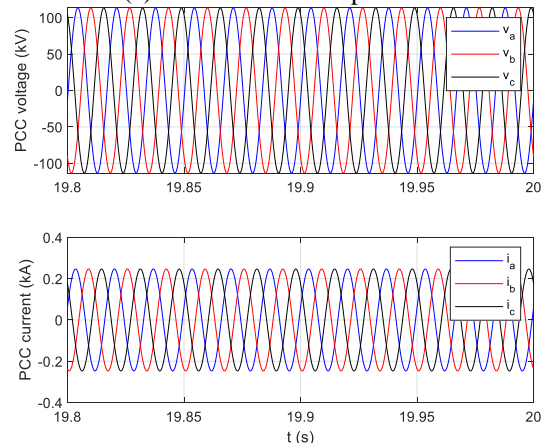
By analyzing these sensitivity matrices, the most significant component, which is most sensitive to the system stability, could be identified.

TABLE I
SYSTEM PARAMETERS

	Symbol	Value	
GFM/GFL inverter power rating	P_{rated}	100 MW	
GFM/GFL inverter rated voltage	V_{rated}	138 kV	
GFM/GFL inverter circuit parameters	R_c	0.367 Ω	
	L_c	0.05 H	
P-f droop gain	M_p	0.05 p.u.	
Q-V droop gain	M_q	0.05 p.u.	
GFL inverter PLL	Case1	k_{ppll}	30
		k_{ipll}	400
	Case2	k_{ppll}	30
		k_{ipll}	165
GFL inverter current PI controller	k_{pc}	0.05	
	k_{ic}	12.5	
GFM inverter voltage PI controller	k_{pv}	0.05	
	k_{iv}	1	



(a) Real and reactive powers.



(b) Voltage and current at PCC.

Fig. 13. PSCAD simulation result of the GFM inverter on Bus 4.

IV. CASES STUDY

In this section, a modified IEEE 14-bus power system [21] as well as a reduced 240-bus WECC system [26] are used to carry out different cases study and verify the proposed stability analysis tool.

Fig. 6 shows a modified IEEE 14-bus power system with multiple IBRs. In the system, there are three GFM inverters connected to Bus 2, 3 and 4, respectively; one GFL inverter connected to Bus 9; and three ideal IVSSs connected to Bus 1, 6 and 8, respectively.

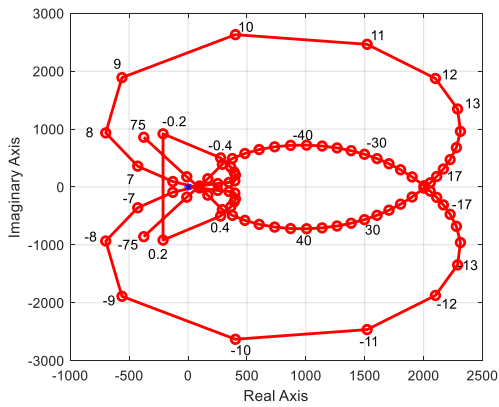
For easy implementation, GFM and GFL inverter models are built in PSCAD with adjustable parameters, and the control schemes of the GFL and GFM inverters are shown in Fig. 7, respectively.

Moreover, the corresponding sequence impedance/admittance models of the GFL and GFM inverters are measured using the method discussed in Section II.B. Two different cases are studied on the modified IEEE 14-bus system and the GFM and GFL inverters' parameters are shown in Table I.

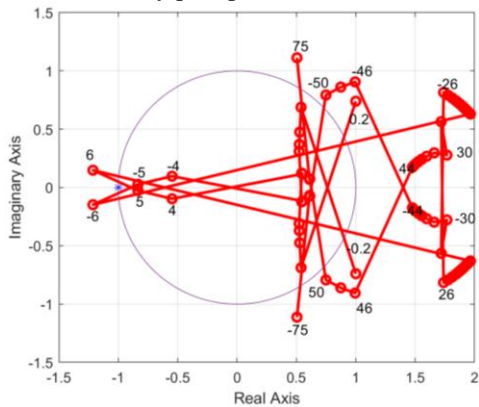
Case 1: IEEE 14-bus power system (unstable system)

In this case, the IEEE 14-bus power system is simulated in PSCAD with the parameters shown in Table I. The system is

> REPLACE THIS LINE WITH YOUR MANUSCRIPT ID NUMBER (DOUBLE-CLICK HERE TO EDIT) <



(a) Nyquist plot of $\det(\mathbf{F})$.



(b) Nyquist plot of eigenvalue of \mathbf{L} .

Fig. 14. Analysis result with determinant- and eigenvalue-based methods.

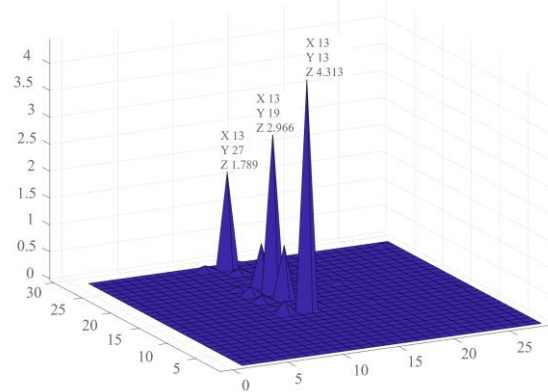
unstable and presents oscillations in the entire system. Fig. 8 shows the performance of the GFL inverter on Bus 9. The d- and q-axis currents of the GFL inverter are shown in Fig. 8(a), respectively, in which the obvious oscillations around 5 Hz can be observed. Fig. 8(b) shows the voltage and current at PCC, which also demonstrates that the system is unstable.

Fig. 9 shows the performance of the GFM inverter on Bus 4. Fig. 9(a) shows the real and reactive powers of the GFM inverter, respectively. The powers also present obvious oscillations around 5 Hz. Fig. 9(b) shows the unstable voltage and current at PCC.

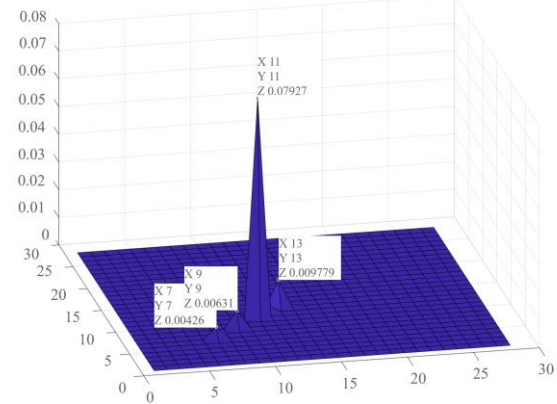
Figs. 10 and 11 show the stability analysis results using the determinant- and eigenvalue-based methods, respectively. Fig. 10 shows that the Nyquist plot of $\det(\mathbf{F})$ encircles the critical point $(0, j0)$ clockwise once, which indicates that the system is unstable. Due to manuscript page number limitations, only one Nyquist plot of a critical eigenvalue of \mathbf{L} is shown in Fig. 11. The figure not only shows that the Nyquist plot encircles the critical point $(-1, j0)$ clockwise once, which indicate the system is unstable; but also displays that the plot crosses the unit circle at around 5 Hz and indicate the system will have oscillations around 5 Hz.

Case 2: IEEE 14-bus power system (stable system)

In this case, only the parameters of the phase-locked loop (PLL) of the GFL inverter are changed as shown in Table I, and



(a) Converter impedance matrix \mathbf{G}_{cd} .



(b) Network impedance matrix \mathbf{G}_{nw} .

Fig. 15. Sensitivity analysis of unstable resonance mode.

all other parameters keep the same as in case 1. With the modified parameters, the power system can operate stably.

Fig. 12 shows the performance of the GFL inverter on Bus 9. Fig. 12(a) shows the d- and q-axis current of the GFL inverter, respectively. All the currents can track their references after a small period of oscillations. Fig. 12(b) shows the voltage and current at PCC, which indicate that the system could operate stably.

Fig. 13 shows the performance of the GFM inverter on Bus 4. Fig. 13(a) shows the real and reactive powers of the GFM inverter, respectively, which indicates that the GFM inverter can provide constant powers in this case. Fig. 13(b) shows the voltage and current at PCC, which also illustrates that the system is stable.

Fig. 14 shows the determinant- and eigenvalue-based stability analysis results, respectively. The figure shows that neither the Nyquist plot of $\det(\mathbf{F})$ nor the Nyquist plot of the eigenvalue of \mathbf{L} encircles their critical points, which indicates the system is stable.

Case 3: Sensitivity analysis of IEEE 14-bus system

In this case study, the sensitivity analysis proposed is conducted for Case 1. Firstly, the eigenvalues of return ratio matrix $\mathbf{L}(s)$ around the resonance frequency are listed in Table II. From this table, the unstable value eigenvalue at resonance frequency is identified. It is observed that the 5th eigenvalue, $-1.2621 + 0.0930j$, is the closest one to the critical point $(-1, 0)$. Then, the left and right eigenvectors of $\mathbf{L}(s)$, u_5 and w_5 can be

> REPLACE THIS LINE WITH YOUR MANUSCRIPT ID NUMBER (DOUBLE-CLICK HERE TO EDIT) <

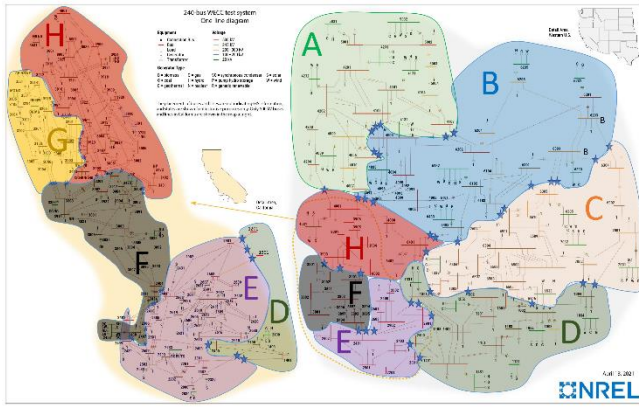


Fig.16. Reduced 240-bus WECC model [26].
calculated accordingly. Thus, the sensitivity matrix of each element of \mathbf{G}_{cd} on the 5th eigenvalue of \mathbf{L} can be calculated as

$$\frac{\partial \mathbf{L}}{\partial \mathbf{G}_{cdij}} = \mathbf{u}_5^T \frac{\partial \mathbf{G}_{cd}}{\partial \mathbf{G}_{cdij}} \mathbf{G}_{nw} \mathbf{w}_5 \quad (19)$$

The absolute value of each element of the sensitivity matrix is plotted in Fig. 15(a). The (13,13) element has the largest value and it indicates that the unstable eigenvalue is most sensitive to the (13,13) element of \mathbf{G}_{cd} . Moreover, it is found that the (13,13) element of \mathbf{G}_{cd} represents the GFL inverter connected to bus 9.

Likewise, the sensitivity matrix of each element of \mathbf{G}_{nw} on the 5th eigenvalue of $\mathbf{L}(s)$ can be calculated as

$$\frac{\partial \mathbf{L}}{\partial \mathbf{G}_{nwij}} = \mathbf{u}_n^T \mathbf{G}_{cd} \frac{\partial \mathbf{G}_{nw}}{\partial \mathbf{G}_{nwij}} \quad (20)$$

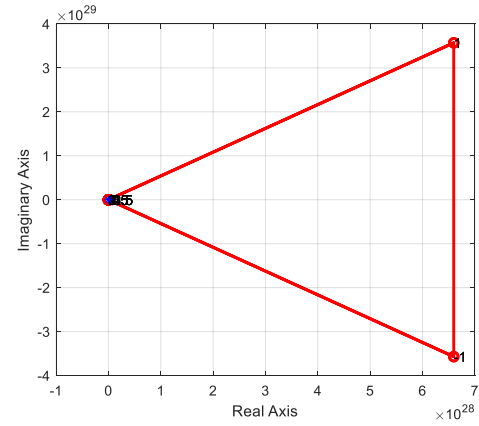
And the absolute value of each element of the sensitivity matrix is plotted as in Fig. 15(b). It is observed that the (11,11) element has the largest value, which indicates that the unstable eigenvalue is most sensitive to the (11,11) element of \mathbf{G}_{nw} . And this element represents the self-admittance of bus 4.

Based on the above-mentioned sensitivity analysis, the transformer between bus 4 and bus 9 is identified as the significant component of the system, which is most sensitive to the overall system stability. Furthermore, the whole system becomes stable by reducing the leakage impedance of the transformer to one third of its original value.

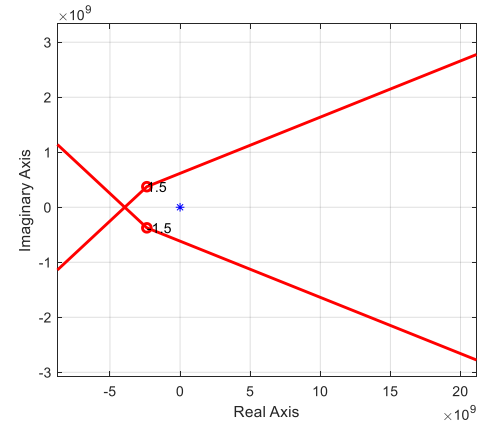
TABLE II

Eigenvalues of return ratio matrix $\mathbf{L}(s)$ at 6 Hz

1	3.4248 + 0.9108i	15	0.0096 + 0.0114i
2	3.2788 - 1.1434i	16	0.0095 - 0.0081i
3	2.0787 + 0.5217i	17	0.0072 + 0.0066i
4	1.9674 - 0.6695i	18	0.0064 + 0.0048i
5	-1.2621 + 0.0930i	19	0.0071 - 0.0044i
6	0.5803 + 0.1780i	20	0.0026 + 0.0031i
7	0.5404 - 0.2293i	21	0.0064 - 0.0035i
8	0.3618 + 0.1950i	22	0.0022 + 0.0006i
9	0.0177 + 0.0527i	23	0.0041 + 0.0005i
10	0.0180 - 0.0424i	24	0.0027 - 0.0026i
11	0.0238 + 0.0267i	25	0.0039 - 0.0006i
12	0.0237 - 0.0192i	26	0.0021 - 0.0007i
13	3.4248 + 0.9108i	27	0.0008 + 0.0000i
14	3.2788 - 1.1434i	28	0.0008 - 0.0000i



(a) Nyquist plot of $\det(\mathbf{F})$.



(b) Zoomed-in view.

Fig. 17. Stability analysis result of 24-bus WECC system with determinant-based method.

Case 4: Reduced 240-bus WECC system (stable system)

The proposed stability analysis tool is also applied to a reduced 240-bus WECC system model, shown in Fig 16: an electromagnetic transient (EMT) timescale system model developed by NREL [26]. To the authors' knowledge, this is the only known example of an open-source, interconnection-scale EMT-timescale model that also embeds IBR dynamics. It represents the generation mix of the actual WECC system in the year of 2018. The reduced 240-bus WECC model is comprised of ~240 buses, 231 traditional generators and 232 renewable generators. The model can represent a range of 20%-90% renewable penetration levels depending on its load condition.

Based on the stability analysis tool presented in the previous sections, firstly, the network model \mathbf{NTFM} is obtained by considering the specification of the 240-bus WECC system, including power rating, voltage rating, loads, transmission lines, source on each bus, etc. Secondly, the impedance models of all the traditional generations as well as IBRs are measured. Then, the 240-bus WECC system is constructed to be MIMO feedback system, and the proposed stability analysis method is applied to do the stability analysis.

Fig. 17 shows the results of the stability analysis of the system. Fig. 17(a) and (b) show the Nyquist plot of $\det(\mathbf{F}(s))$ and the zoom-in view around the critical point, respectively. It is

> REPLACE THIS LINE WITH YOUR MANUSCRIPT ID NUMBER (DOUBLE-CLICK HERE TO EDIT) <

observed that the Nyquist plot of $\det(\mathbf{F}(s))$ does not encircle critical point $(0, j0)$ clockwise, which indicates the reduced 240-bus WECC system is stable, and the stability analysis result is also consistent to its PSCAD simulation result.

V. CONCLUSION

The impedance-based stability analysis tool using black-box model is developed in this paper to analyze bulk power systems with a high penetration level of IBRs. The procedure of conducting stability analysis and sensitivity analysis of the power system is presented in detail. Different cases based on a modified IEEE 14-bus power system and a reduced 240-bus WECC system are studied to validate the effectiveness of the proposed methods. The analysis results show that both the determinant- and eigenvalue-based methods are capable of determining whether or not the overall system is stable. Moreover, the eigenvalue-based method could further predict the system's oscillation frequency, as well as identify the system component that is most sensitive to the overall system stability.

REFERENCES

- [1] Shah, Shahil, et al. "Impedance Methods for Analyzing Stability Impacts of Inverter-Based Resources: Stability Analysis Tools for Modern Power Systems." *IEEE Electrification Magazine*, vol. 9, no. 1, pp. 53-65, Mar. 2021.
- [2] P. Kundur, *Power System Stability and Control*. New York: McGraw-Hill, 1994.
- [3] I. Kamwa, "Using MIMO system identification for modal analysis and global stabilization of large power systems," *2000 Power Engineering Society Summer Meeting (Cat. No.00CH37134)*, 2000, pp. 817-822 vol. 2, doi: 10.1109/PSS.2000.867459.
- [4] W. Du, Q. Fu and H. Wang, "Open-Loop Modal Coupling Analysis for a Multi-Input Multi-Output Interconnected MTDC/AC Power System," in *IEEE Transactions on Power Systems*, vol. 34, no. 1, pp. 246-256, Jan. 2019, doi: 10.1109/TPWRS.2018.2857857.
- [5] L. Ding, X. Lu and J. Tan, "Small-Signal Stability Analysis of Low-Inertia Power Grids with Inverter-Based Resources and Synchronous Condensers," *2022 IEEE Power & Energy Society Innovative Smart Grid Technologies Conference (ISGT)*, 2022, pp. 1-5.
- [6] Y. Zhou *et al.*, "Small-signal Stability Analysis of Power Systems under Uncertain Renewable Generation," *2022 IEEE Power & Energy Society General Meeting (PESGM)*, 2022, pp. 1-5, doi: 10.1109/PESGM48719.2022.9916873.
- [7] Y. Pan *et al.*, "Towards the Robust Small-Signal Stability Region of Power Systems Under Perturbations Such as Uncertain and Volatile Wind Generation," in *IEEE Transactions on Power Systems*, vol. 33, no. 2, pp. 1790-1799, March 2018, doi: 10.1109/TPWRS.2017.2714759.
- [8] K. W. Wang, C. Y. Chung, C. T. Tse and K. M. Tsang, "Multimachine eigenvalue sensitivities of power system parameters," in *IEEE Transactions on Power Systems*, vol. 15, no. 2, pp. 741-747, May 2000.
- [9] L. Yang, Z. Xu, J. Østergaard, Z. Y. Dong, K. P. Wong and X. Ma, "Oscillatory Stability and Eigenvalue Sensitivity Analysis of A DFIG Wind Turbine System," in *IEEE Transactions on Energy Conversion*, vol. 26, no. 1, pp. 328-339, March 2011.
- [10] J. Chen and J. Chen, "Stability Analysis and Parameters Optimization of Islanded Microgrid With Both Ideal and Dynamic Constant Power Loads," in *IEEE Transactions on Industrial Electronics*, vol. 65, no. 4, pp. 3263-3274, April 2018.
- [11] R. D. Middlebrook, "Input filter considerations in design and application of switching regulators," in *Proc. IEEE Ind. Appl. Soc. Annu. Meeting*, 1976.
- [12] B. Wen, D. Dong, D. Boroyevich, R. Burgos, P. Mattavelli, and Z. Shen, "Impedance-based analysis of grid-synchronization stability for three-phase paralleled converters," *IEEE Trans. Power Electron.*, vol. 31, no. 1, pp. 26-38, Jan. 2016.
- [13] M. Amin and M. Molinas, "Small-Signal Stability Assessment of Power Electronics Based Power Systems: A Discussion of Impedance- and Eigenvalue-Based Methods," *IEEE Transactions on Industry Applications*, vol. 53, no. 5, pp. 5014-5030, Sept.-Oct. 2017.
- [14] Y. Liao and X. Wang, "Impedance-Based Stability Analysis for Interconnected Converter Systems with Open-Loop RHP Poles," *IEEE Transactions on Power Electronics*, vol. 35, no. 4, pp. 4388-4397, April 2020.
- [15] Y. Li *et al.*, "Stability Analysis and Location Optimization Method for Multiconverter Power Systems Based on Nodal Admittance Matrix," *IEEE Journal of Emerging and Selected Topics in Power Electronics*, vol. 9, no. 1, pp. 529-538, Feb. 2021.
- [16] W. Cao, "Impedance-based Stability Analysis and Controller Design of Three-phase Inverter-based AC Systems," Ph.D. dissertation, University of Tennessee, Knoxville, 2017.
- [17] N. Cifuentes, M. Sun, R. Gupta and B. C. Pal, "Black-Box Impedance-Based Stability Assessment of Dynamic Interactions Between Converters and Grid," *IEEE Transactions on Power Systems*, vol. 37, no. 4, pp. 2976-2987, July 2022.
- [18] K. W. Wang, C. Y. Chung, C. T. Tse and K. M. Tsang, "Multimachine eigenvalue sensitivities of power system parameters," in *IEEE Transactions on Power Systems*, vol. 15, no. 2, pp. 741-747, May 2000.
- [19] Y. Li, Z. Shuai, Y. Peng, J. Shen and Y. Hong, "Eigenvalue Sensitivity of Stability Analysis for a Droop Controlled Inverter," 2018 IEEE Energy Conversion Congress and Exposition (ECCE), Portland, OR, USA, 2018, pp. 4148-4154.
- [20] D. Sun, H. Liu and M. Gong, "A Stability Analysis Tool for Bulk Power Systems Using Black-Box Models of Inverter-based Resources," 2022 IEEE Industry Applications Society Annual Meeting (IAS), 2022, pp. 1-6.
- [21] J. Grainger and W. Stevenson, "Power system analysis," New York: McGraw-Hill, 1994, pp. 238-280.
- [22] S. Shah, P. Koralewicz, V. Gevorgian and R. Wallen, "Sequence Impedance Measurement of Utility-Scale Wind Turbines and Inverters – Reference Frame, Frequency Coupling, and MIMO/SISO Forms," *IEEE Transactions on Energy Conversion*, vol. 37, no. 1, pp. 75-86, March 2022.
- [23] H. Liu, H. Guo, J. Liang and L. Qi, "Impedance-Based Stability Analysis of MVDC Systems Using Generator-Thyristor Units and DTC Motor Drives," *IEEE Journal of Emerging and Selected Topics in Power Electronics*, vol. 5, no. 1, pp. 5-13, March 2017.
- [24] Illinois Center for a Smarter Electric Grid. (2013). [Online]. Available FTP: <http://publish.illinois.edu/smartergrid/>
- [25] S. Skogestad and I. Postlethwaite, "Multivariable feedback control: analysis and design," Hoboken, NJ: John Wiley, 2nd edition, 2005, pp.113-150.
- [26] Wang, Bin, Richard Wallace Kenyon, and Jin Tan. Developing a PSCAD Model of the Reduced 240-Bus WECC Test System: Preprint. N.p., 2022. Print.